ISSN (Print) 1226-1750
ISSN (Online) 2233-6656
Journal of Magnetics 25(2), 254-261 (2020) https://doi.org/10.4283/JMAG.2020.25.2.254

Heat and Mass Transfer in Magneto-Newtonian Fluid Past a Paraboloid of Revolution with Internal Heat Source

Naveed Ahmed[1], Adnan[2], Umar Khan[3], Syed Tauseef Mohyud-Din[4], Ilyas Khan[5]*, and Kottakkaran Sooppy Nisar[6]

[1]*Department of Mathematics, Faculty of Sciences, HITEC University Taxila Cantt, Pakistan*
[2]*Department of Mathematics, Mohi-ud-Din Islamic University, Nerian Sharif, Azad Jammu and Kashmir, Pakistan*
[3]*Department of Mathematics and Statistics, Hazara University, Mansehra, Pakistan*
[4]*University of Multan, Multan, Pakistan*
[5]*Faculty of Mathematics and Statistics, Ton Duc Thang University, Ho Chi Minh City, Vietnam*
[6]*Department of Mathematics, College of Arts and Sciences, Prince Sattam bin Abdulaziz University, Wadi Aldawaser, 11991, Saudi Arabia*

(Received 7 December 2018, Received in final form 8 May 2020, Accepted 8 May 2020)

The objectives of the research are to explored the heat and mass transport over a paraboloid surface of revolution by taking the effects of Lorentz force, resistive heating and internal heat source. The dimensionless version of the model was attained via similarity transformations. Then, for solution purpose, RK scheme is utilized and performed computations for the flow fields. The influence of different physical quantities on the flow characteristics described comprehensively via graphs. It is examined that the stretching index parameter m opposes the fluid velocity and the temperature enhances for Eckert number. Moreover, significant impacts of the Schmidt number are observed for mass transfer gradient.

Keywords : newtonian fluid, paraboloid of revolution, ohmic heating, internal heat source

1. Introduction

The heat and mass transfer in streamline flow of viscous incompressible fluid under the influence of Lorentz force, resistive heating and heat generation/absorption over a paraboloid surface of revolution is received much interest of the researchers. Such flows extensively exist over a bullet and bonnet of the vehicles.

The magnetized laminar flow is significant from industrial applications point of view. These are in solar collectors, aeronautical engineering and magnetospheres. Therefore, the analysis of magnetized flows attained much interest of the researchers due to significant uses in various industries like oil purification, pumps and production of heat exchangers etc.

The flow of Newtonian as well as non-Newtonian fluids is significant over a paraboloid surface of revolution. Therefore, the researchers turned their attentions towards the analysis of such flows by incorporating the influence of applied magnetic field, radiative heat flux, resistive heating, internal heat source, thermophoretic and Brownian motion parameter in the constitutive governing models.

Recently, Reddy *et al.* [1] were reported the flow characteristics over a paraboloid surface of revolution. They explored the impacts of viscous dissipation in the flow behavior of Fe_3O_4-Casson nanofluid over a convective geometry and made comprehensive discussion based on the reported results. Moreover, they computed the numeric results for the shear stresses and local rate of heat transfer. In 2017, Koriko *et al.* [2] was perceived the flow of micropolar fluid over a paraboloid geometry for autocatalytic chemical reaction. They found the similarity solutions for the model and analyzed the velocity and temperature behavior via graphs. Ajayi *et al.* [3] was explored the boundary layer for Casson fluid over a paraboloid geometry by incorporating the effects of viscous dissipation and radiative heat flux. The theoretical analysis for the flow of Carreau and Casson fluids in the existence of heat generation/absorption over a paraboloid geometry was discussed in [4]. The comparison for the

*Corresponding author: Tel: +92-332-8902728
Fax: +92-992-392188, e-mail: ilyaskhan@tdtu.edu.vn

velocity and temperature was made in the presented work for various flow quantities.

Recently, Abegunrin *et al.* [5] perceived the flow behavior of Eyring Powell fluid over a revolving paraboloidal sheet. The study is conducted in the presence of chemical reaction effects. Crane [6] was perceived the flow past a stretchable surface. They comprehensively reported the flow field under the variations of different parameters. Later on, the effects of various parameters on the heat and mass transfer were described in [7]. The flow characteristics over a continuously stretchable and rotating surfaces was presented in [8] and [9], respectively. They perceived the impacts of an interesting parameter λ in the flow field that is the quotient of rotating surface to the stretching rate of the surface. In 2006, Sharidan *et al.* [10] explored the unsteady Falkner flow over a porous surface. The influence of concentration gradients in three-dimensional flow over radiative sheet was examined by Reddy *et al.* [11]. They discussed the influence of Lorentz force, internal heat source and thermophoretic parameter in the flow fields. The heat transfer analysis for the flow over a porous stretchable surface, magnetized flow over a bi-laterally stretching surface, the flow behavior of unsteady dissipative flow of non-Newtonian fluid and unsteady flow of Casson fluid past a stretching surface by incorporating the effects of thermal radiations, slip and convective boundary conditions were perceived in [12-15], respectively. The Casson fluid characteristics past an inclined stretchable plane described [16]. The influence of thermal radiations and chemical reaction are focused in his study. Furthermore, useful analysis for the Newtonian as well as non-Newtonian fluids under various flow conditions in different geometries was perceived in [17-29]. The flow characteristics in the occurrence of dissipative effects were perceived in [30]. Heat and mass transfer inspection in magnetized Walter's B type nanofluid, analysis of micropolar nanofluid, second law analysis for power law fluid, bioconvection flow of Jeffery nanofluid and impacts of induced magnetic field for CuO/H_2O nanofluid perceived in [31-35].

2. Model Formulation

The 2D steady laminar flow of Newtonian fluid is taken over a paraboloid surface of revolution. The influence of an imposed magnetic field, resistive heating and internal heat source are also taken in the governing model. It is assumed that the fluid flow in the region $A(x+b)^{\frac{1-m}{2}} \le y < \infty$. Moreover, the fluid flow with velocity $U_w = \dfrac{U_0}{(x+b)^{-m}}$, at the surface where, U_0 is the stretching rate and m denotes the velocity stretching parameter that is < 1 for upper paraboloid surface of revolution. The physical flow scenario is decorated in Fig. 1. Physical Theme .

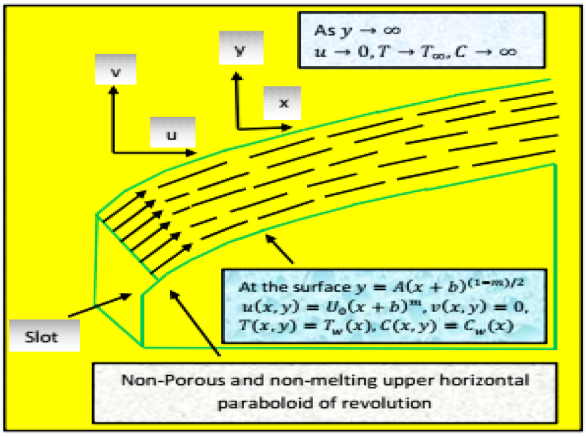

(a)

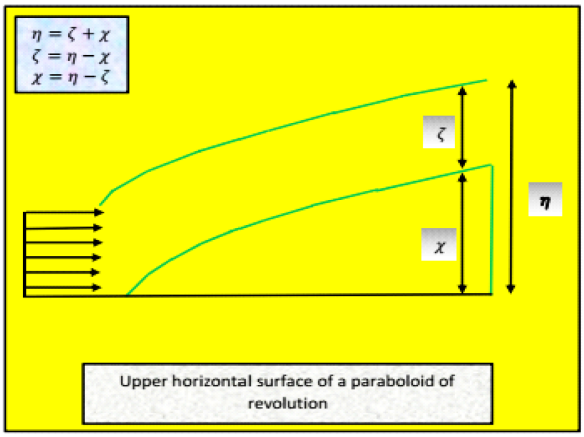

(b)

Fig. 1. (Color online) Physical Theme.

The magneto-radiative governing model by taking the effects of heat generation/absorption is described by the following set of equations [36]:

$$\frac{\partial u}{\partial x} + \frac{\partial v}{\partial y} = 0\,, \tag{1}$$

$$u\frac{\partial u}{\partial x} + v\frac{\partial u}{\partial y} = \frac{\mu}{\rho}\left(\frac{\partial^2 u}{\partial y^2}\right) - \frac{\sigma B^2}{\rho}u\,, \tag{2}$$

$$u\frac{\partial T}{\partial x} + v\frac{\partial T}{\partial y} = \frac{k}{\rho c_p}\left(\frac{\partial^2 T}{\partial y^2}\right) + \frac{Q_0(T_\infty - T_0)}{\rho c_p}$$

$$(2.7128)^{-ny\sqrt{\frac{m+1}{2}}\sqrt{\frac{U_0}{\nu}}(x+b)^{\frac{m-1}{2}}} + \frac{\sigma B^2}{\rho c_p}(u^2)\,, \tag{3}$$

$$u\frac{\partial C}{\partial x} + v\frac{\partial C}{\partial y} = D\left(\frac{\partial^2 C}{\partial y^2}\right). \tag{4}$$

The equation of continuity is described in Eq. (1). The law of conservation of energy and mass are incorporating in Eqs. (2)-(4), respectively. Furthermore, the velocity components u and v are aligned horizontally and vertically, respectively. The fluid density is represented by ρ, μ denotes the dynamic viscosity, specific heat is denoted by c_p, k is the thermal conductivity, σ is electrical conductivity, B^2 is applied magnetic field, T is the fluid temperature, C is the fluid concentration and D denotes the mass diffusivity.

The related set of particular flow conditions is:

At $y = 0$:

$$u = U_w,\ v = 0,\ T = T_w(x),\ C = C_w(x), \tag{5}$$

At $y \to \infty$:

$u \to 0$, $T \to T_\infty$, $C \to C_\infty$, where, u, v and T are functions of x and y. (6)

The supporting similarity transformations for the model are defined in the following manner:

$$\left.\begin{aligned} u = \frac{\partial \psi}{\partial y},\ v = -\frac{\partial \psi}{\partial x} \\ \psi(x,y) = \sqrt{\frac{2\nu U_0}{m+1}}(x+b)^{\frac{m+1}{2}} f(\eta) \\ \eta = \sqrt{\frac{(m+1)U_0}{2\nu}}(x+b)^{(m-1)/2} y \\ \beta^*(\eta) = \frac{T - T_\infty}{T_w - T_\infty} \\ \phi^*(\eta) = \frac{C - C_\infty}{C_w - C_\infty} \end{aligned}\right\}. \tag{7}$$

Where, ψ denotes the stream function and chosen in such a way that it satisfies the continuity equation:

$$u = U_0(x+b)^m f'(\eta), \tag{8}$$

$$v = -\sqrt{\frac{2\nu U_0}{(m+1)}}\frac{(m+1)}{2}(x+b)^{\frac{(m-1)}{2}} f(\eta). \tag{9}$$

After plugging the similarity variables in the governing model, the following form is attained:

$$f''' - \left(\frac{2m}{m+1}\right)f'^2 + ff'' - M^2 f' = 0, \tag{10}$$

$$\beta^{*\prime\prime} - \left(\frac{m-1}{m+1}\right)Pr\,\eta f' \beta^{*\prime} + \frac{2\mathrm{Pr}\gamma_1}{(m+1)}(2.7128)^{-n\eta} + \frac{2\mathrm{Pr}EcM^2}{(m+1)}f'^2 = 0, \tag{11}$$

$$\phi^{*\prime\prime} - \left(\frac{m-1}{m+1}\right)Sc\,\eta f' \phi^{*\prime} + Scf\phi^{*\prime} = 0. \tag{12}$$

For the self-similar boundary conditions, it is very noteworthy to mention that the lower value of y is not at the initial point of the slot. Therefore, it is not possible to impose all the conditions in Eq. (5) at $y = 0$. By using $y = A(x+b)^{(1-m)/2}$ minimal value of y is almost corresponds to the minimal value of the similarity variable η. This value is given in the following formula:

$$\eta = A\sqrt{\frac{(m+1)U_0}{2\nu}} = \chi. \tag{13}$$

Thus, feasible flow conditions at the wall for suitable scale are $\eta = \chi$. Therefore, the boundary conditions become:

$$f'(\chi) = 1, f(\chi) = \chi\left[\frac{1-m}{1+m}\right],\ \beta^*(\chi) = 1,\ \phi^*(\chi) = 1, \tag{14}$$

$$f'(\chi) \to 0,\ \beta^*(\chi) \to 0,\ \phi^*(\chi) \to 0. \tag{15}$$

Furthermore, nondimensional flow model given Eqs. (10)-(12) depends on the similarity variable η. on the other hand, auxiliary conditions in Eqs. (14) and (15) are depending on variable χ. To set the domain $[\chi, \infty)$ to $[0, \infty)$, it is suitable to chose $F(\zeta) = F(\eta - \chi) = f(h)$, $\beta(\zeta) = \beta(\eta - \chi) = \beta^*(\eta)$, and $\phi(\zeta) = \phi(\eta - \chi) = \phi^*(\eta)$. Finally, the Eqs. (10)-(12) transformed into the following form:

$$F''' - \left(\frac{2m}{m+1}\right)(F'^2 + FF'' + M^2 F') = 0, \tag{16}$$

$$\beta'' - \left(\frac{m-1}{m+1}\right)Pr\,\eta F'\beta' + \mathrm{Pr}F\beta' + \frac{2Pr\gamma_1}{(m+1)}(2.7128)^{-n\zeta} + \frac{2PrEcM^2}{(m+1)}F'^2 = 0, \tag{17}$$

$$\phi'' - \left(\frac{m-1}{m+1}\right)Sc\,\eta F'\phi' + ScF\phi' = 0. \tag{18}$$

The self-similar boundary conditions for flow model are the following:

At $\zeta = 0$:

$$F'(\zeta) = 1,\ F(\zeta) = \chi\left[\frac{1-m}{1+m}\right],\ \beta(\zeta) = 1,\ \phi(\zeta) = 1, \tag{19}$$

At $\zeta \to \infty$:

$$F'(\zeta) \to 0,\ \beta(\zeta) \to 0,\ \phi(\zeta) \to 0. \tag{20}$$

The dimensionless physical quantities embedded in the Eqs. (16)-(18) are magnetic parameter M, Prandtl number

Pr, Eckert number *Ec* and Schmidt number *Sc*. Mathematical expressions for these parameters are as under:

$$M^2=\frac{\sigma B_0^2}{\rho},\ Pr=\frac{\nu\rho C_p}{k},\ Ec=\frac{U_0(x+b)^{m+1}}{c_p(T_w-T_\infty)}\ \text{and}\ Sc=\frac{\nu}{D}.$$

Further, nondimensional formulas for the quantities of physical and engineering interest are as under:

$$\left.\begin{aligned} C_F\sqrt{Re_x}&=F''(0)\\ Nu(Re_x)^{-\frac{1}{2}}&=-\beta'(0)\\ Sh(Re_x)^{-\frac{1}{2}}&=-\phi'(0)\end{aligned}\right\}. \tag{21}$$

Where, $Re_x=\dfrac{U_w(x+b)}{\nu}$ is local Reynolds number.

3. Mathematical Analysis

The model under consideration is nonlinear boundary value problem defined at semi-infinite interval. In such situation it is very difficult to handle the model approximately or not even exists such solutions. Therefore, numerical techniques are useful for such models. Thus, we turned toward the numerical computations of the model. For this, we employed the coupling of Runge-Kutta scheme with shooting technique [37-39]. In order to initiate the algorithm, firstly nonlinear BVP is transform into the IVP. For this, the transformations are introduced:

$$y_1=F,\ y_2=F',\ y_3=F'',\ y_4=\beta,\ y_5=\beta',$$
$$y_6=\phi,\ y_7=\phi'. \tag{22}$$

The coupled system given by Eqs. (16)-(18) can be rewritten in the following version:

$$F'''=\left(\frac{2m}{m+1}\right)F'^2-FF''+M^2F', \tag{23}$$

$$\beta''=\left(\frac{m-1}{m+1}\right)Pr\,\eta F'\beta'-PrF\beta'-\frac{2Pr\gamma_1}{(m+1)}(2.7128)^{-\zeta\eta}-\frac{2PrEcM^2}{(m+1)}F'^2, \tag{24}$$

$$\phi''=\left(\frac{m-1}{m+1}\right)Sc\,\eta F'\phi'-ScF\phi'. \tag{25}$$

By plugging the transformations, we attained the following form the model:

$$\begin{bmatrix}y_1'\\y_2'\\y_3'\\y_4'\\y_5'\\y_6'\\y_7'\end{bmatrix}=\begin{bmatrix}y_2\\y_3\\\left(\frac{2m}{m+1}\right)y_2^2-y_1y_3+M^2y_2\\y_5\\\left(\frac{m-1}{m+1}\right)Pr\left[\eta y_2y_5-y_1y_5-\frac{2\gamma_1}{(m+1)}(2.7128)^{-\zeta\eta}-\frac{2EcM^2}{(m+1)}y_2^2\right]\\y_7\\\left(\frac{m-1}{m+1}\right)Sc\,\eta y_2y_7-Scy_1y_7\end{bmatrix}, \tag{26}$$

The supporting initial conditions are as follows:

$$\begin{bmatrix}y_1\\y_2\\y_3\\y_4\\y_5\\y_6\\y_7\end{bmatrix}=\begin{bmatrix}1\\\chi\left[\frac{1-m}{1+m}\right]\\l_1\\1\\l_2\\1\\l_3\end{bmatrix}. \tag{27}$$

Where, l_i (for i = 1, 2, 3) are unknown which are computed by using the software Mathematica 10.0.

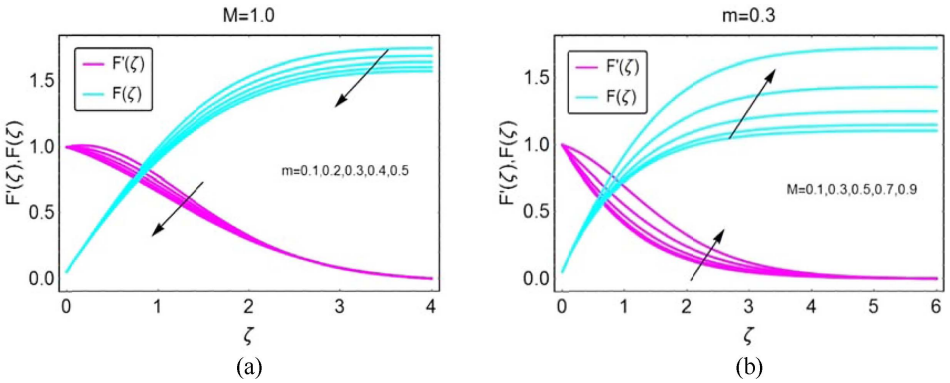

(a) (b)

Fig. 2. (Color online) The variations of (a) *m* and (b) *M* on the velocity field.

4. Graphical Results

This section is devoted to explore the flow characteristics against the various preeminent flow quantities.

Figures 2a and 2b portraying the fluid vertical and horizontal velocities against the multiple values of m and magnetic number M, respectively. Figure 2a elaborates the effects of varying velocity stretching index parameter m on the velocity profiles. It is perceived that the velocity drops. The horizontal velocity $F'(\zeta)$ is decreases rapidly in the region $0.1 \le \zeta \le 1.0$. For $\zeta > 1.0$, the decrement in the fluid velocity becomes gradually slow for higher velocity stretching index parameter. The vertical velocity profile $F(\zeta)$ is also decreasing function of stretching index parameter m. In the vicinity of the paraboloid surface of revolution the effects of the stretching parameter are almost inconsequential. Beyond the region $\zeta > 3$, these effects are noted maximum and the velocity profile becomes straight for increasing values of velocity stretching index parameter.

The effects of Lorentz forces on the fluid velocities (both vertical and horizontal velocity) are portrays in Fig. 2b. It is perceived that the imposed magnetic field favors the fluid velocity. The horizontal velocity of the fluid increases rapidly in the region $0.0 \le \zeta \le 2.0$. On the other hand, vertical component of the fluid velocity shows almost inconsequential variations in the locality of the paraboloid of revolution. For $\zeta > 3.0$, these variations are maximum and the vertical velocity profile becomes almost straight. Three-dimensional view of the vertical velocity $F(\zeta)$ and horizontal velocity $F'(\zeta)$ are elucidated in Figs. 3a and 3b, respectively.

The impacts of Ec and the velocity stretching index m on the fluid temperature $\beta(\zeta)$ and temperature gradient $\beta'(\zeta)$ are depicted in Figs. 4a and 4b, respectively. The effects of Eckert number on the fluid temperature are very prominent. Fluid temperature increases rapidly near the paraboloid of revolution. The maximum fluid temperature is perceived in the portion $0.0 \le \zeta \le 5.0$. Beyond this region, increase in the fluid temperature becomes slow

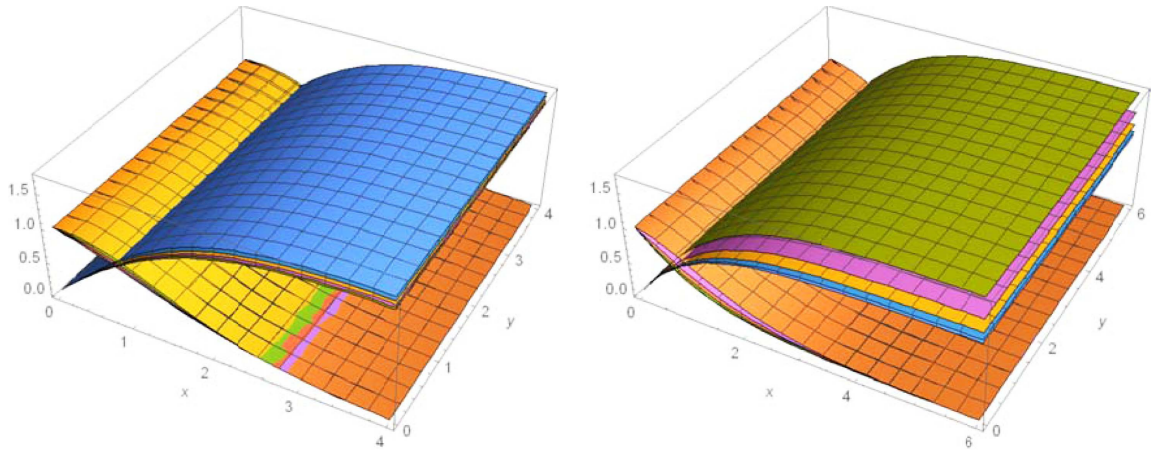

Fig. 3. (Color online) 3D view for (a) m and (b) M on the velocity field.

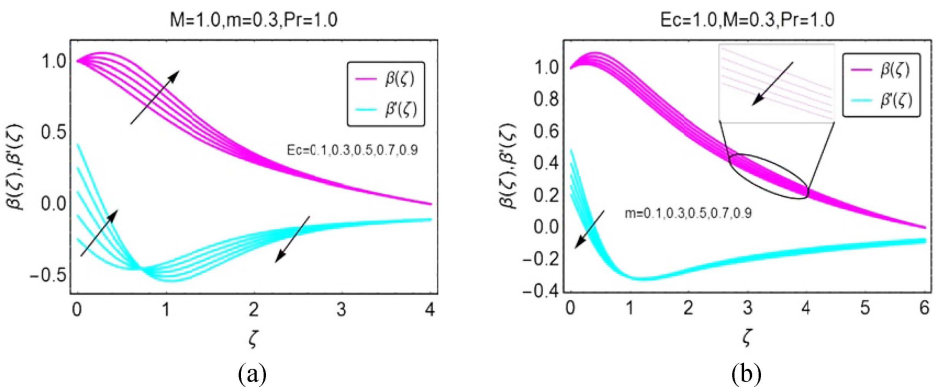

Fig. 4. (Color online) The variations of (a) Ec and (b) m on $\beta(\zeta)$ and $\beta'(\zeta)$.

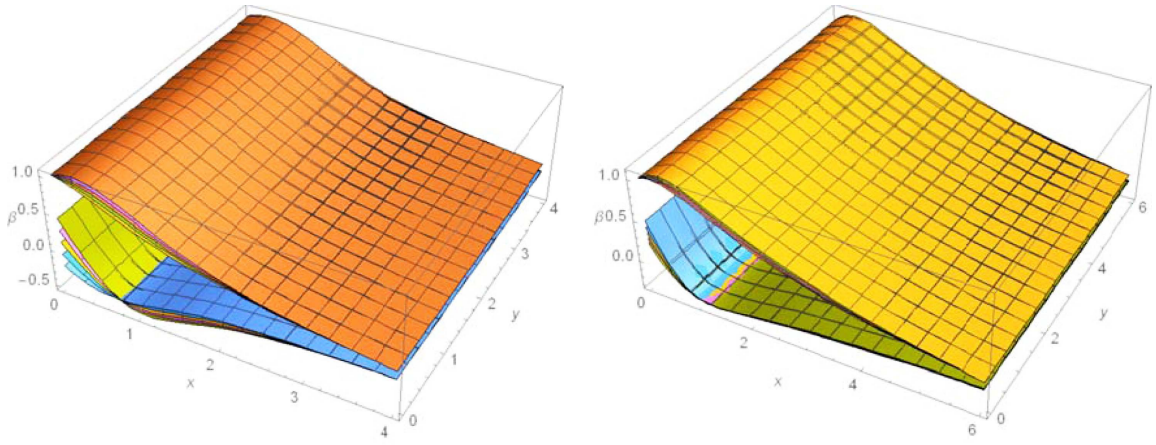

(a) (b)

Fig. 5. (Color online) 3D view of $\beta(\zeta)$ and $\beta'(\zeta)$ for (a) *Ec* and (b) *m*.

down for higher Eckert number. Far from the surface, the effects of Eckert number become almost inconsequential and the fluid temperature vanishes asymptotically. Further, the thermal gradient $\beta'(\zeta)$ is an increases for more dissipative fluid in the portion $0.0 \le \zeta \le 1.0$. On the other hand, the impact of velocity stretching index parameter *m* on dimensionless fluid temperature $\beta(\zeta)$ demonstrated in Fig. 4b. It is noted that the velocity starching index parameter opposes the fluid temperature. Near the surface very cleared effects of *m* on $\beta(\zeta)$ are perceived. The fluid

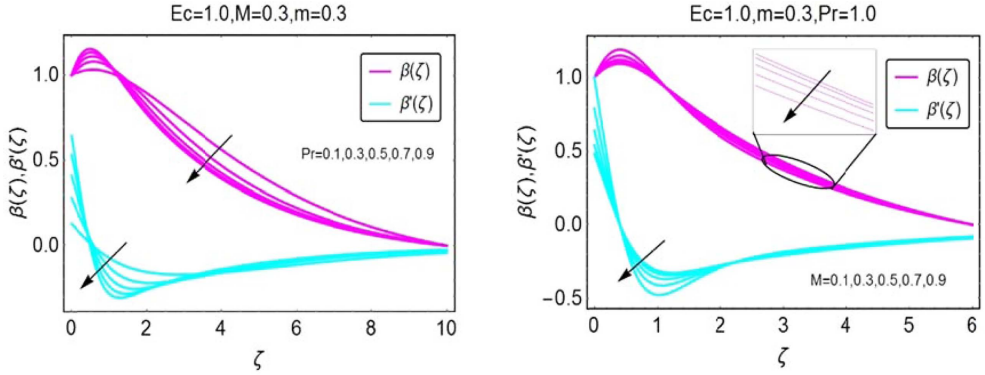

(a) (b)

Fig. 6. (Color online) The variations of (a) *Pr* and (b) *M* on $\beta(\zeta)$ and $\beta'(\zeta)$.

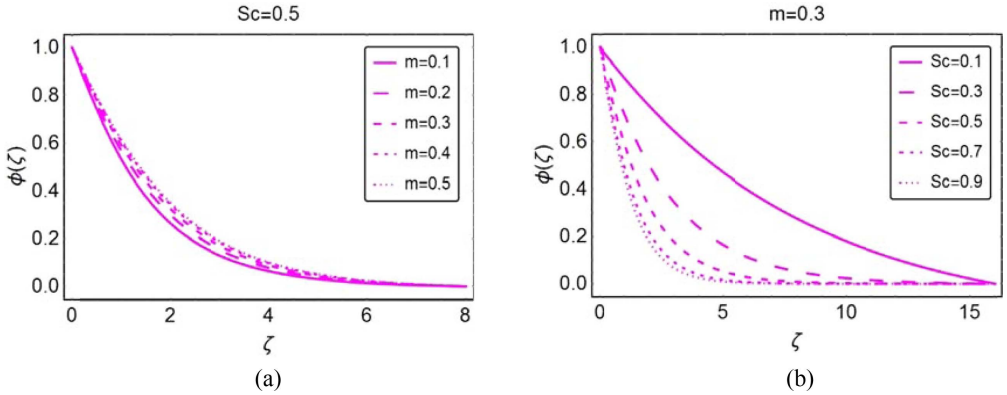

(a) (b)

Fig. 7. (Color online) The variations of (a) *m* and (b) *Sc* on $\phi(\zeta)$.

Table 1. The numerical values for $F''(0)$, $-\beta'(0)$ and $-\phi'(0)$.

m	M	Pr	Ec	Sc	$F''(0)$	$-\beta'(0)$	$-\phi'(0)$
0.1	0.3	0.3	0.3	0.3	–0.74408	0.10263	0.39599
0.2					–0.80526	0.11671	0.38380
0.3					–0.85440	0.12895	0.37416
0.1	0.5				–0.68476	0.00575	0.41974
	0.7				–0.49025	0.01468	0.44304
	0.9				–0.17212	0.02451	0.48151
	0.3	0.5				–0.14031	–
		0.7				–0.27717	–
		0.9				–0.40666	–
		0.3	0.5			–0.00202	–
			0.7			–0.00464	–
			0.9			–0.00725	–
			0.3	0.5			0.56660
				0.7			0.72646
				0.9			0.87936

temperature gradually decreases for smaller values of the velocity stretching index parameter. Three-dimensional scenario of $\beta(\zeta)$ for varying Eckert number and the velocity stretching index parameter m portrayed in Figs. 5a and 5b, respectively.

Figures 6a and 6b, decorating the behavior of fluid temperature by varying the Prandtl number and magnetic number, respectively. From these, it can be seen that the fluid temperature decreases for arising Prandtl number and magnetic parameter. For stronger magnetic field, the thermal profile shows rapid decreasing behavior near the surface. As we move away from the surface, the effects of these parameters become almost inconsequential and temperature of the fluid vanishes asymptotically.

The variations in the concentration field of the fluid for stretching index parameter m and Schmidt number Sc are elaborated in Figs. 7a and 7b, respectively. It is noted that for arising values of stretching index m, the concentration of the fluid starts increasing and maximum increment is examined in the region $0.0 \le \zeta \le 4.0$. On the other hand, the Schmidt parameter opposes the fluid concentration. For higher Sc, the concentration field $\phi(\zeta)$ decreases promptly between $\zeta = 0.0$ to $\zeta = 10.0$. Furthermore, for higher ζ the fluid concentration $\phi(\zeta)$ shows asymptotic behavior.

The numerical values of the shear stresses, local nusselt and Sherwood numbers for varying pertinent physical parameters are given in Table 1. It is noted that for higher values of stretching index parameter m, the skin friction coefficient increases absolutely while, stronger magnetic field opposes it. The presence of resistive heating lead to increase in the local rate of heat transfer. The arising values of Schmidt number favor the fluid concentration and stretching index parameter m opposes it.

Table 2. Comparative analysis for $F''(0)$ [40].

m	Animasaun and Sandeep [40]	Present
0.1	–0.8671009	–0.8681133
0.2	–0.8654053	–0.859491
0.3	–0.8584863	–0.852225

Table 2 highlighted the comparative analysis for various values of parameter n. From the comparison, it is examined that the presented results are acceptable and showed an excellent agreement with the existing literature results. This comparison showed the accuracy and validity of the analysis.

5. Conclusions

The magnetized flow of Newtonian fluid is taken over a paraboloid surface of revolution. The influences of Ohmic heating are also incorporated in the energy equation. It is examined that:

i. The velocities of the fluid enhance due to the stretching index n.

ii. The temperature of the fluid rises for more viscous fluid.

iii. The temperature drops for more magnetized fluid and increasing Pr opposes the fluid temperature.

iv. The concentration field declines by increasing the Schmidt parameter.

v. The local heat transfer rate significantly enhances for stronger magnetic field.

vi. The mass transport is rises for higher values of the Schmidt number.

References

[1] R. J. V. Reddy, V. Sugunamma, and N. Sandeep, J. Mol. Liq. **229**, 380 (2017).
[2] O. K. Korik and I. L. Animasaun, Front. Heat Mass Trans. **8**, 26 (2017).
[3] T. M. Ajayi, A. J. Omowaye, and I. L. Animasaun, J. Appl. Math. 2017 (2017). https://doi.org/10.1155/2017/1697135.
[4] G. Kumaran, N. Sandeep, and I. L. Animasaun, Alex. Eng. J. **57**, 3 (2018).
[5] O. A. Abegunrin, I. L. Animasaun, and N. Sandeep, Alex. Eng. J. **57**, 3 (2018).
[6] L. J. Crane, J. Appl. Math. Phys. **21**, 645 (1970).
[7] P. S. Gupta and A. S. Gupta, Cand. J. Chem. Eng. **55**, (1977).
[8] L. G. Grubk and K. M. Booba, J. Heat Trans ASME. **107**, 248 (1985).
[9] C. Wang, ZAMP **39**, 177 (1988).
[10] S. Sharidan, N. Amin, and I. Pop, Int. Heat Tech. **25**, 111 (2006).
[11] P. S. Reddy and A. J. Chamkha, J. Appl. Fluid Mech. **9**, 2443 (2016).
[12] I. Ahmad, M. Ahmad, and M. Sajid, Therm. Sci. **20**, 1913 (2016).
[13] I. Ahmad, Z. Abbas, and M. Sajid, Therm. Sci. **15** (2011).
[14] I. Ullah, I. Khan, and S. Shafie, Sci. Rep. **7** (2017). doi: 10.1038/s41598-017-01205-5.
[15] I. S. Oyelakin, S. Mondal, and P. Sibanda, Alex. Eng. J. **55**, 1025 (2016).
[16] P. B. A. Reddy, Ain. Shams. Eng. J. **7**, 593 (2016).
[17] S. Sharidan and T. Mahmood, Int. J. Appl. Mech. Eng. **11**, 647 (2006).
[18] Aurangzaib, A. R. M. Kasim, N. F. Mohammad, and S. Shafie, World Appl. Sci. J. **21**, 766 (2013).
[19] M. Jonnadula, P. Polarapu, M. G. Reddy, and M. Venakateswarlu, Procedia. Eng. **127**, 1315 (2015).
[20] M. Sheikholeslami and K. Vajravelu, Appl. Math. Comput. **298**, 272 (2017).
[21] A. Gul, I. Khan, and S. Shafie, Nanoscale. Res. Lett. (2015).
[22] S. T. Mohyud-Din, U. Khan, N. Ahmed, and S. M. Hassan, Appl. Sci. **5** (2015).
[23] M. Sheikholeslami, T. Hayat, and A. Alsaedi, Int. J. Heat. Mass. Trans. **106**, 745 (2017).
[24] S. Aman, I. Khan, Z. Ismail, and M. Z. Salleh, Neural. Comput. Appl. **30**, 789 (2016).
[25] I. Ullah, S. Shafie, I. Khan, and J. King, Saud Univ. Sci. **29**, 250 (2016).
[26] N. Athirah, M. Zin, I. Khan, and S. Shafie, J. Mol. Liq. **222**, 138 (2016).
[27] M. Sheikholeslami and S. A. Shehzad, Int. J. Heat. Mass. Trans. **106**, 1261 (2017).
[28] M. Sheikholeslami, Eur. Phys. J. Plus. **132** (2017).
[29] A. Gul, I. Khan, S. Shafie, A. Khalid, and A. Khan, PLoS One. **11**, 1 (2015).
[30] S. Saleem, S. Nadeem, and C. S. K. Raju, Microsyst. Technol. **25** (2019).
[31] S. Saleem, H. Firdous, S. Nadeem, and A. U. Khan, Arab. J. Sci. Eng. **44** (2019).
[32] M. A. Sadiq, A. U. Khan, S. Saleem, and S. Nadeem, RSC. Adv. **9** (2019).
[33] M. A. E. Aziz and S. Saleem, Entropy. **21**, 5 (2019).
[34] S. Saleem, H. Rafiq, A. A. Qahtani, M. A. E. Aziz, and M. Y. Malik, Math. Probl. Eng. 2019 (2019).
[35] I. L. Animasaun, B. Mahanthesh, A. O. Jagun, T. D. Bankole, S. Ramachandran, N. A. Shah, and S. Saleem, T. Heat. Trans. **141**, 2 (2019).
[36] I. L. Animasaun, Alex. Eng. J. **55**, 3 (2019).
[37] U. Khan, N. Ahmed, and S. T. Mohyud-Din, Appl. Therm. Eng. **113**, 1107 (2017).
[38] J. A. Khan, M. Mustafa, T. Hayat, and A. Alsaedi, PLoS One. **9** (2014).
[39] B. Mahanthesh, B. J. Gireesha, and R. S. R. Gorla, J. Assoc. Arab Univ. Basic Appl. Sci. **23**, 75 (2016).
[40] I. L. Animasaun and N. Sandeep, Powder Tech. **301** (2016).